The Effect of NMDA Receptors on Gain Modulation

Michiel Berends
michiel@tnb.ua.ac.be
Reinoud Maex
reinoud@tnb.ua.ac.be
Erik De Schutter
erik@tnb.ua.ac.be
Laboratory of Theoretical Neurobiology, Born-Bunge Foundation, University of Antwerp, Antwerp B-2610, Belgium

The ability of individual neurons to modulate the gain of their input-output function is important for information processing in the brain. In a recent study (Mitchell & Silver, 2003), shunting inhibition was found to modulate the gain of cerebellar granule cells subjected to simulated currents through AMPA receptor synapses. Here we investigate the effect on gain modulation resulting from adding the currents mediated by NMDA receptors to a compartmental model of the granule cell. With only AMPA receptors, the changes in gain induced by shunting inhibition decreased gradually with the average firing rate of the afferent mossy fibers. With NMDA receptors present, this decrease was more rapid, therefore narrowing the bandwidth of mossy fiber firing rates available for gain modulation. The deterioration of gain modulation was accompanied by a reduced variability of the input current and saturation of NMDA receptors. However, when the output of the granule cell was plotted as a function of the average input current instead of the input firing frequency, both models showed very similar response curves and comparable gain modulation. We conclude that NMDA receptors do not directly impair gain control by shunting inhibition, but the effective bandwidth decreases as a consequence of the increased total charge transfer.

1 Introduction

Gain modulation (GM) is a powerful computational principle that has been proposed to be operative in several brain functions, like sensory processing, attention modulation, and the computation of coordinate transformations (Salinas & Thier, 2000). The central mechanism of computation by GM is the transformation of the gain, that is, the slope of the input-output (IO) curve of neurons. This is a multiplicative operation on the IO curve and expresses an altered sensitivity of the neuron to changes in its input. In contrast, a translation of the IO curve is an additive operation and can be

computationally useful to subtract a certain baseline activity. It has been shown both theoretically and experimentally using the dynamic-clamp technique that GM can be controlled at the level of a single neuron through the influence of a parameter such as the level of background firing (Burkitt, Meffin, & Grayden, 2003; Chance, Abbott, & Reyes, 2002; Fellous, Rudolph, Destexhe, & Sejnowski, 2003; Kuhn, Aertsen, & Rotter, 2004) or shunting inhibition (Doiron, Longtin, Berman, & Maler, 2000; Mitchell & Silver, 2003; Prescott & De Koninck, 2003).

What effect does a change in the level of shunting inhibition have on the IO curve of a neuron when it is excited by injecting constant currents of various magnitudes? The increased membrane conductance reduces the slope of the relationship between the magnitude of the subthreshold input current and the membrane voltage, in accordance with Ohm's law ($I = gV$). This would suggest also that the suprathreshold relationship between the input strength and the firing rate of the neuron might scale multiplicatively. However, it has been shown that with stimulation by constant input currents, only a translation of the IO curve results from changing the level of shunting inhibition (Holt & Koch, 1997).

GM can be obtained when noise, which, for instance, arises from background synaptic inputs, is added to the injected current (Chance et al., 2002). Neurons like pyramidal cells receive background firing from a large number of small-amplitude excitatory and inhibitory synapses. By increasing the overall levels of excitation and inhibition, both the variance of the background input and the average membrane conductance are increased, and the slope of the IO curve is reduced. If excitation and inhibition are kept in approximate balance, it is possible to obtain an almost perfect multiplicative transformation, that is, without an additive component.

In a similar manner, shunting inhibition can also generate GM if the cell is driven by varying synaptic input (Mitchell & Silver, 2003). In this case, both the noise and the excitatory drive to the cell arise from the same source: the synaptic inputs. The transformation of the IO curve by shunting inhibition also has in this case, apart from a multiplicative component, an additive component, which results from the altered excitation-inhibition ratio.

To attain a significant modulation of the gain, both a large change of the amount of shunting inhibition and a high level of the input noise are required. In cerebellar granule cells (GCs), the amount of shunting inhibition can reach a considerable size. GCs receive phasic inhibition from a small number of Golgi cells (2–10; see Jakab & Hamori, 1988). The inhibition evoked by Golgi cell spikes consists of a fast, direct component and a much slower spillover component (Rossi, Hamann, & Attwell, 2003). In addition, GCs receive tonic inhibition that is independent of Golgi cell firing (for a review, see De Schutter, 2002). The strength of this tonic inhibition can be modulated by acetylcholine (Rossi et al., 2003) and reach several times its baseline value, implying that the gain of GCs can be regulated independent of the firing rate of Golgi cells.

Gain modulation by shunting inhibition has been demonstrated in GCs receiving simulated synaptic inputs in a dynamic-clamp approach (Mitchell & Silver, 2003). A high level of input noise was ensured here by the fact that GCs have only a small number of input channels—four mossy fibers (MFs)— and that the simulated excitatory postsynaptic currents (EPSCs) had a large peak amplitude in addition to their fast rise and decay time constants, corresponding to the AMPA receptor component of synaptic transmission. However, the dynamic-clamp protocol did not simulate the currents mediated by NMDA receptors (D'Angelo, Rossi, & Taglietti, 1993; Silver, Traynelis, & Cull-Candy, 1992), which have an important role in long-term potentiation of the MF–GC synapse (D'Angelo, Rossi, Armano, & Taglietti, 1999).

In this study, we investigated the effect of NMDA receptors on gain modulation using a conductance-based model of the GC. NMDA receptors have much slower kinetics than AMPA receptors, which might affect the level of input noise. The long activation times of NMDA receptors make their share in the total charge transfer substantial, despite their small contribution to the peak EPSP amplitude (D'Angelo, De Filippi, Rossi, & Taglietti, 1995).

2 Methods

2.1 The Model Granule Cell. The present conductance-based model of a rat cerebellar GC at 37°C is an elaboration of previous models (D'Angelo et al., 2001; Gabbiani, Midtgaard, & Knopfel, 1994; Maex & De Schutter, 1998). Its single compartment has a diameter of 10 μm and a specific membrane capacitance of 1 μF/cm^2. The membrane conductance consisted of a GABA-independent component of 200 pS with a reversal potential of -60 mV (D'Angelo et al., 2001), and a GABA-dependent component with a reversal potential of -65 mV. The baseline level of the GABA-dependent conductance was set at 200 pS, in accordance with the estimated value of the tonic extrasynaptic GABA$_A$ conductance in the absence of acetylcholine (Hamann, Rossi, & Attwell, 2002; Rossi et al., 2003). In the presence of acetylcholine, the extrasynaptic GABA$_A$ conductance can increase to several times its baseline level (Rossi et al., 2003). The total amount of tonic inhibition to a GC is further increased by the spillover inhibition mentioned above and can reach values over 1 nS. In our simulations, we investigated the effect of a GABA-dependent tonic inhibition of 1200 pS (baseline level $+1$ nS).

The model contained eight types of active membrane channels: a fast Na$^+$ channel, a delayed rectifier K$^+$ channel, an A-type K$^+$ channel, a high-voltage-activated Ca^{2+} channel, and a Ca^{2+}-activated K$^+$ channel, all as implemented before (Maex & De Schutter, 1998) but with their voltage dependency shifted by $+5$ mV and with $\bar{g}_{NAF} = 0.04$ S/cm^2 and $\bar{g}_{KA} = 0.004$ S/cm^2. We added a persistent Na$^+$ channel and a slow K$^+$ channel, taken from D'Angelo et al. (2001), and an inwardly rectifying noninactivating K$^+$ channel, constructed after experimental data from D'Angelo et al. (1995) and Rossi, De Filippi, Armano, Taglietti, & D'Angelo (1998).

This inward rectifier had a peak conductance of $9.5 \, 10^{-4} \, \text{S/cm}^2$ and was activated with a forward rate $\alpha = 0.4 \, e^{-0.08(Vm+86.3)}(\text{ms}^{-1})$ and a backward rate $\beta = 0.4 \, e^{0.04(Vm+86.3)}(\text{ms}^{-1})$. The inward rectifier, having an equilibrium potential of -84 mV, dominated the membrane conductance at rest, leading to a resting membrane potential of -76.9 mV (Cathala, Brickley, Cull-Candy, & Farrant, 2003; D'Angelo et al., 2001). The rheobase current I_{rheo} (the current at which firing starts) was 8 pA in the absence of GABA-mediated inhibition. At this level of input current, the spike threshold measured approximately -39 mV (Cathala et al., 2003; D'Angelo et al., 1995).

2.2 The Synapses. GCs receive excitatory input from on average four MFs (Ito, 1984) through synapses containing both AMPA receptors (AMPARs) and NMDA receptors (NMDARs) (Silver et al., 1992). MFs can fire at very high rates; for example, tonic firing levels up to 200 Hz have been measured in monkeys during eye and limb movements (Kase, Miller, & Noda, 1980; van Kan, Gibson, & Houk, 1993) and during passive vestibular stimulation (Goldberg & Fernandez, 1971). Therefore, we used in this study a large range of MF input rates, from 0 to 200 Hz. We modeled the MF input by four independent Poisson processes. As instantaneous firing rates of MFs can exceed 800 Hz (Eccles, Faber, Murphy, Sabah, & Taborikova, 1971; Garwicz, Jorntell, & Ekerot, 1998), we did not include a dead time.

The kinetics of the AMPARs were described by a rise time constant of 0.08 ms and three decay time constants of 0.37 ms, 2.2 ms, and 15 ms, contributing 80%, 16%, and 4% to the peak conductance, respectively (DiGregorio, Nusser, & Silver, 2002). Because of their fast kinetics, saturation of the AMPARs is negligible and was not taken into account.

GCs have both synaptic and extrasynaptic NMDA receptors. The kinetics of the NMDAR in this study were based on NMDAR currents measured after single release events (D'Angelo, Rossi, & Taglietti, 1994; Rossi et al., 2002), and were described by a 10% to 90% rise time of about 5 ms and two decay time constants of 17 ms (contributing 60%) and 69 ms (40%), after correction for temperature using a Q_{10} factor of 2. The actual behavior during high-frequency stimulation is less well known. The relative synaptic and extrasynaptic contributions to the current (77% versus 23% after a single stimulus event; Rossi et al., 2002) might change, resulting in different overall kinetics. Subsequent synaptic events, following shortly after the first, will elicit less increase in the conductance than the first if a significant fraction of the postsynaptic receptors is still occupied due to the first event. Therefore, saturation of NMDARs can occur, as the kinetics of NMDARs are slow. There is evidence that synaptic NMDARs are not saturated by a single release event, and in an experimentally investigated case (Wang, 2000) the saturation level after a single event was estimated to be 31%. In our NMDAR conductance description, we set the saturation after a single event accordingly; we used a ratio of 0.31 between the unitary peak

conductance, $\bar{g}_{NMDA}$, and the maximum conductance when all NMDARs are saturated, g_{sat} ($\bar{g}_{NMDA}$ and g_{sat} denote the conductances in the absence of the Mg^{2+}-block).

The activation of the fast and the slow component of the saturating NMDAR conductance was each modeled using the equations (Drew & Abbott, 2003)

$$dn(t)/dt = T(t)(1 - n(t)) - n(t)/\tau_{decay}$$

$$dT(t)/dt = -T(t)/\tau,$$

where $T(t)$ was increased by T_{peak} after each incoming event. The used constants were, for the fast component, $\tau = 1.5$ ms, $\tau_{decay} = 17$ ms, and $T_{peak} = 0.33$, and, for the slow component, $\tau = 3.5$ ms, $\tau_{decay} = 67$ ms, and $T_{peak} = 0.12$. The total NMDAR conductance was then given by

$$g_{NMDA}(t) = g_{sat}(0.6\, n_{fast}(t) + 0.4\, n_{slow}(t))B(V(t)).$$

The voltage-dependent Mg^{2+}-block is described by $B(V(t)) = 1/(1 + \eta[Mg^{2+}]e^{-\gamma V(t)})$, with $\eta = 0.28$ mM^{-1}, $\gamma = 0.062$ mV^{-1}, and $[Mg^{2+}] = 1.2$ mM (Jahr & Stevens, 1990). The AMPAR peak conductance was set to 732 pS (DiGregorio et al., 2002). The effect of NMDARs on the IO relationship of GCs was explored using NMDAR-to-AMPAR peak conductance ratios of 0.0, 0.64 (Rossi et al., 2002), and 1.28 (Gabbiani et al., 1994). For both excitatory synaptic currents, the reversal potential was 0 mV. Figures 1A and 1B show the excitatory postsynaptic potentials (EPSPs) and currents (EPSCs) in these different configurations (N0, N64, and N128). The contribution of the NMDAR current to the peak of the EPSP and the ratio of the peak of the NMDAR current versus the peak of the AMPAR current most closely resembled experimental values in configuration N128 (D'Angelo et al., 1995; Silver et al., 1992).

All simulations were done in Neuron 5.5 (Hines & Carnevale, 1997) and extended over a mimimum period of 30 s. Numerical integration was done with the Crank-Nicolson method using a time step of 0.02 ms.

3 Results

We investigated the effect of 1 nS shunting inhibition on the average firing rate $\langle f_{GC} \rangle$ of the model GC during stimulation of the MFs at various average firing rates $\langle f_{MF} \rangle$. We compared the influence of NMDARs on the gain (defined as $\text{Gain}(\langle f_{MF} \rangle) = d\langle f_{GC} \rangle / d\langle f_{MF} \rangle$), for three levels of the NMDAR peak conductance (see section 2).

In the presence of NMDAR currents the overall gain of GCs, quite expectedly, considerably increased (see Figures 2A to 2C; note the different scales
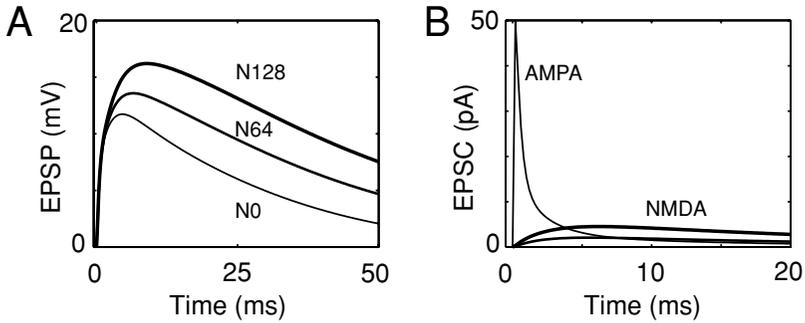
Figure 1: Unitary EPSPs and EPSCs in the granule cell model from a holding potential of −70 mV. (A) EPSPs for configurations N0, N64, and N128. Peak of the EPSP in N0: 11.85 mV; in N64: 13.7 mV with the NMDAR contribution to the peak 13.5%; in N128: 16.3 mV with the NMDAR contribution to the peak 27.3%. (B) EPSCs with separated AMPAR and NMDAR components. The AMPAR-mediated current is approximately equal in all three configurations and has a peak of 50 pA. In configuration N64, the NMDAR-mediated current (lower line) has a peak of 2.1 pA (4.2% of the peak of the AMPAR component). In configuration N128, the NMDAR current (upper line) has a peak of 4.5 pA (9.1% of the AMPAR peak current).

of the ordinate axes). The rise in overall gain was accompanied by a comparable rise of the average input current $\langle I \rangle$ to the cell (see Figure 2E). The gain in configuration N0 without shunting inhibition increased slightly with the average input frequency but was close to linear (see Figure 2A). With the addition of NMDAR currents, the relation became increasingly convex (see Figures 2B and 2C), except at low input frequencies, where it stayed almost linear. This convex behavior was not a consequence of the refractory period of the GC, which is known to reduce in integrate-and-fire neurons the slope of the input-output curve at high firing rates (Bugmann, 1991), since the IO relationship plotted as a function of the average input current $\langle I \rangle$ did not show a similar slope reduction within the same range of GC firing rates (see Figure 3A). Therefore, the reduced slope at high input frequencies must be attributed to saturation of the NMDAR-mediated current (see below).

Upon application of 1 nS shunting inhibition, both additive and multiplicative modification of the IO curve could be discerned (see Figures 2A to 2C). In the model lacking NMDARs, the IO curve had a strongly concave shape in the low-frequency range and became gradually more linear at high input frequencies (see Figure 2A). The presence of NMDARs reduced the extent of the concave part of the curve (see Figures 2B and 2C). To quantify the effect of shunting inhibition on the gain, we defined a gain modulation index: $I_{GM} = (\text{Gain}_{control} - \text{Gain}_{shunting})/\text{Gain}_{control}$. Figure 2D shows the behavior of I_{GM} as a function of the input frequency for the three synaptic
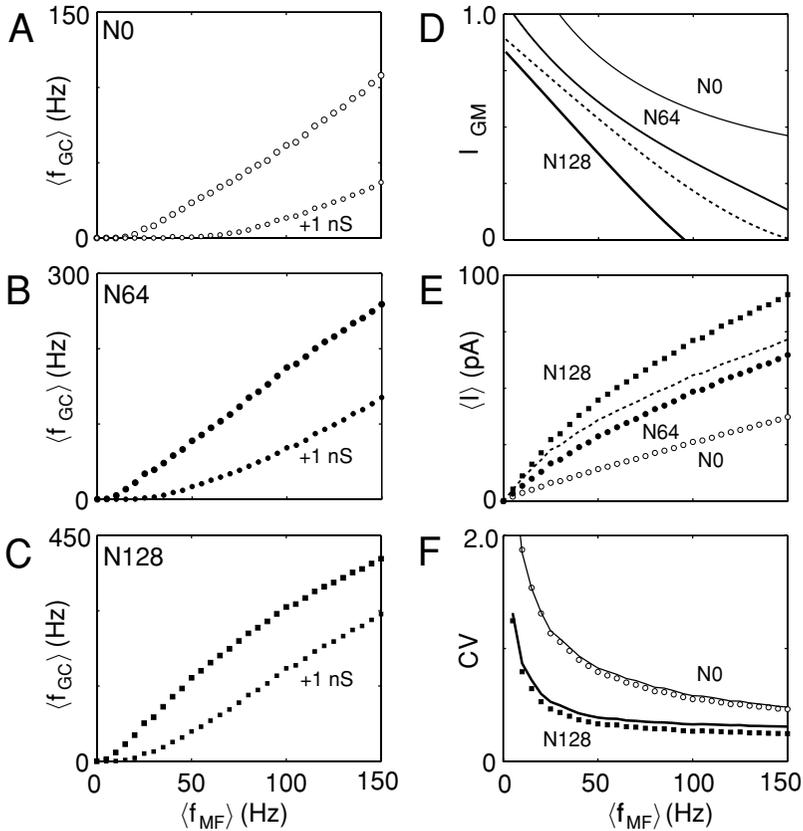
Figure 2: The effect of 1 nS shunting inhibition on the gain of the granule cell model, expressed as a function of the average MF firing rate $\langle f_{MF} \rangle$. (A–C) Average granule cell firing rate $\langle f_{GC} \rangle$ in configuration N0 (A, open circles), N64 (B, closed circles), and N128 (C, closed squares) for control (large symbols) and 1 nS shunting inhibition (small symbols). (D) Gain modulation index I_{GM} (see text) in four different synaptic configurations: N0, N64, N128, and the configuration with $\bar{g}_{NMDA}/\bar{g}_{AMPA} = 1.28$ and $\bar{g}_{NMDA}/g_{sat} = 0.62$ (dashed lines). (E) Average synaptic input current $\langle I \rangle$ for the same configurations as in D. Control curves and curves in the presence of 1 nS shunting inhibition (not shown) almost completely overlapped. (F) Coefficient of variation of the total synaptic conductance (CV_g) in configuration N0 (thin solid line) and configuration N128 (thick solid line) and of the corresponding excitatory synaptic input current (CV_I, N0: open circles, N128: closed squares). In configuration N0, CV_g could be well fitted with a function of the form $a e^b$, yielding $a = 12.12$ and $b = -0.50$ ($R^2 > 0.99$).
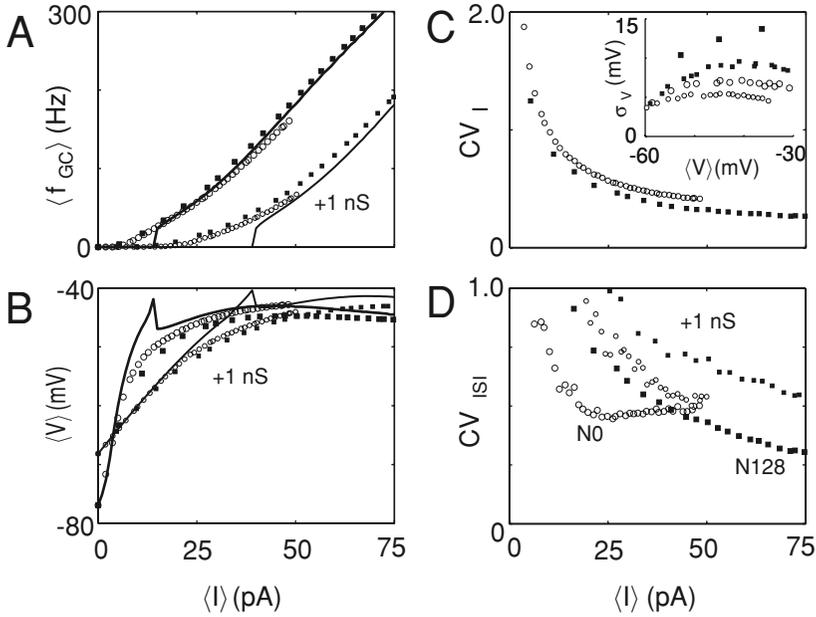
Figure 3: The effect of 1 nS shunting inhibition on the gain of the granule cell model, expressed as a function of the average input current $\langle I \rangle$. (*Curve styles as in Figures 2A and 2C. For clarity, the curves corresponding to the N64 configuration were omitted.*) (A) Average granule cell firing rate $\langle f_{GC} \rangle$ for configurations N0 and N128 and for excitation by constant input currents in the control case (thick solid line) and with 1 nS shunting inhibition (thin solid line). (B) Average membrane potential $\langle V \rangle$ for the same configurations as in *A.* (C) CV of the input current for configurations N0 and N128 in the control case. Control curves and curves in the presence of 1 nS shunting inhibition (not shown) almost completely overlapped. Inset: Standard deviation of the membrane potential fluctuations versus average membrane potential in the granule cell with all eight active membrane conductances blocked for configurations N0 and N128 in the control case and with 1 nS shunting inhibition. (D) CV of the interspike intervals of the granule cell for configurations N0 and N128 in the control case and with 1 nS shunting inhibition.

configurations of Figures 2A to 2C. With only AMPARs, 1 nS shunting inhibition resulted in an I_{GM} greater than 0.45 over the whole frequency range, while in the presence of NMDARs, I_{GM} dropped below 0.45 at high MF firing rates (at $\langle f_{MF} \rangle = 78$ and 43 Hz in the case of N64 and N128, respectively). Hence, GM was reduced in the presence of NMDARs, and particularly at high input frequencies, this reduction was profound. Simulations with shunting inhibition levels of 500 pS and 1500 pS gave qualitatively similar differences between configurations N0, N64, and N128. Therefore,

we conclude that NMDARs reduce the bandwidth of input frequencies at which GM occurs.

To investigate the influence on gain modulation of the ratio between the NMDAR peak conductance and the conductance at full saturation, we constructed a synaptic configuration with the same conductance at full saturation of the NMDARs as in N64, but with the ratio $\bar{g}_{NMDA}/g_{sat} = 0.62$, that is, with the same unitary peak conductance as in N128. This resulted at low input frequencies in a faster rise with input frequency of the NMDAR conductance than in configuration N64, as the steeper slope of the $\langle I \rangle$-$\langle f_{MF} \rangle$ curve indicates (see Figure 2E). The gain modulation index $I_{GM}(f)$ was reduced in this new configuration compared with the N64 case (see Figure 2D).

The influence of the input noise on GM becomes clearer when the firing rate of the GC is plotted as a function of the average input current $\langle I \rangle$ instead of the input frequency $\langle f_{MF} \rangle$.[1] Figure 3A compares for each synaptic configuration this IO curve with the curve obtained by injection of constant input currents I. The rheobase current was 14.5 pA in the control case and 39.5 mV with 1 nS shunting inhibition. As in integrate-and-fire neurons, shunting inhibition resulted in a rightward shift of the f-I curve, but did not lead to modulation of the gain in the absence of fluctuations (Holt & Koch, 1997; Mitchell & Silver, 2003). Indeed, the average subthreshold membrane potential $\langle V \rangle$ scaled multiplicatively on shunting inhibition for $I < I_{\text{rheo}}$ and had a sharp peak at $I = I_{\text{rheo}}$ (see Figure 3B). Note that in our case, $\langle V \rangle$ does not monotonically decrease for $I > I_{\text{rheo}}$, unlike $\langle V \rangle$ in models with a fixed spike threshold and/or strong repolarization level (Doiron et al., 2000). The spike threshold and the repolarization in our model shifted several millivolts upward during high-stimulus intensities (approximately up to 6 mV and 3 mV, respectively).

In contrast, with fluctuating input currents resulting from stochastic synaptic activation, the GC fired also at $I < I_{\text{rheo}}$ (see Figure 3A), resulting in a smoothing of the threshold nonlinearity and a clear GM by shunting inhibition. A complete analytical description of the influence of input noise on the firing rate of a neuron and its role in GM is complex (Burkitt et al., 2003; Ricciardi, 1977; Stein, 1965; Tuckwell, 1988). However, the effect of input noise on the firing rate can be qualitatively understood by considering the relation between the membrane potential fluctuations and the variability of the synaptic input currents.

When a synapse, with instantaneous rise and a single decay time constant τ_s and a fixed peak conductance $\bar{g}$, is activated according to a Poisson process with rate f, the average conductance will be $\langle g \rangle = \bar{g} f \tau_s$, and the variance

---

[1] The average input current $\langle I \rangle$ and voltage $\langle V \rangle$ represent the averages taken when the membrane potential was lower than -35 mV; hence, most of the action potential is filtered out.

is given by $\sigma_g^2 = \bar{g}^2 f \tau_s$, using Campbell's theorem (Rice, 1954; van Kampen, 1981). The coefficient of variation (CV) of the AMPAR conductance of our model GC decreased proportional to $1/\sqrt{\langle f_{MF} \rangle}$, in good agreement with Campbell's theorem (see Figure 2F). The variability of the input currents σ_I^2 closely follows that of the synaptic conductances σ_g^2, when the variations in the driving potential $(V\text{-}E_r)$ of the input current are small (see Figure 2F for a comparison of CV_g and CV_I). The membrane potential is a low-pass filtered version of the input current, and its variance is given by $\sigma_V^2 = \sigma_I^2 \tau_s / g_{tot}^2 (\tau_m + \tau_s)$, where g_{tot} is the total conductance—the membrane conductance and the average synaptic conductance combined (see Chance et al., 2002).

The probability that a membrane potential fluctuation triggers a spike depends on both the amplitude of the fluctuation and the value of the membrane potential, which determines the distance to threshold. In the regime of $\langle I \rangle \leq I_{rheo}$, the average voltage grows with $\langle I \rangle$. Because the standard deviation of the voltage fluctuation also grows with the input levels, the largest effect of fluctuations on the firing rate occurs for amplitudes of $\langle I \rangle$ close to the rheobase current. For $\langle I \rangle > I_{rheo}$, the influence of fluctuations on the firing rate diminishes again. First, there is no further increase in the percentage of time the membrane potential spends close to threshold, as the average membrane potential $\langle V \rangle$ becomes almost independent of $\langle I \rangle$ (see Figure 3B; see also Holt & Koch, 1997). Second, spiking no longer depends solely on fluctuations, as the average input current itself, without fluctuations, causes spiking. Hence, the contribution of fluctuations on the firing rate relative to $\langle I \rangle$ decreases with input frequency, as σ_I grows less than $\langle I \rangle$. Thus, an increase of the input frequency resulted in a transition from a fluctuation-driven regime to a current-driven regime (Doiron et al., 2000; Tiesinga, Jose, & Sejnowski, 2000).

With shunting inhibition, input noise enhanced the firing rate over a larger range of average input currents (see Figure 3A). This can be explained by the slower rise of $\langle V \rangle$ as a function of $\langle I \rangle$ for $\langle I \rangle \leq I_{rheo}$ (see Figure 3B), resulting in a more gradual transition from a fluctuation-driven to a current-driven regime. Moreover, the reduction of the membrane time constant ensures that the cell is faster driven to the asymptotic subthreshold depolarization level, bringing the neuron earlier in a state (Troyer & Miller, 1997), where fluctuations can trigger a spike. This argument holds provided that shunting inhibition does not severely reduce the variability of the membrane potential. It can be shown that this is the case if the effective membrane time constant τ_m is much larger than the synaptic decay time constant τ_s. If the application of shunting inhibition leads to an increase of the intrinsic membrane conductance by a factor m, then the input rate must also increase by m to obtain the same average depolarization $\langle V \rangle$. Therefore, the variance of the input current increases in the presence of shunting inhibition as $\sigma_I^2 \rightarrow m\sigma_I^2$. Because the total conductance increases as $g_{tot} \rightarrow m\, g_{tot}$, while the effective membrane time constant decreases as $\tau_m \rightarrow \tau_m/m$, the variance of the membrane potential fluctuations changes

as $\sigma_V^2 \rightarrow \sigma_V^2(\tau_m + \tau_s)/(\tau_m + m\tau_s)$ (Chance et al., 2002). We investigated the effect of shunting inhibition on the membrane potential fluctuations in the absence of spiking and blocked all the channels in our GC model. As expected, the application of 1 nS shunting inhibition led to only a moderate reduction of σ_V compared to the control value at the same average membrane potential (see the inset in Figure 3C).

The average and variance of the conductance resulting from activation of NMDARs by a Poisson spike train cannot be evaluated using Campbell's theorem, because NMDAR conductances saturate and are dependent on the membrane potential through the Mg^{2+} block. But simulations showed that the CV of the total synaptic conductance decreased faster with input frequency in the presence of NMDARs (see Figure 2F). Thus, as above, the inclusion of NMDARs reduced the input variability as a function of the input frequency.

Surprisingly, but consistent with the almost identical $\langle f_{GC} \rangle$-$\langle I \rangle$ curves for the different synaptic configurations in Figure 3A, the influence of NMDARs on GM as a function of the average input current $\langle I \rangle$ was minimal. Nevertheless, the statistical characteristics of the input currents were not identical in the different synaptic configurations. The inclusion of NMDARs led to a slight reduction of CV_I when average input currents were compared (see Figure 3C), suggesting less influence of fluctuations on the firing rate. However, the temporal correlation of the input current was enlarged, resulting in larger fluctuations of the membrane potential in the model without Hodkin-Huxley channels (see the inset in Figure 3C). As has been shown to be the case for integrate-and-fire neurons (Salinas & Sejnowski, 2002), an increase of the temporal correlation led to a higher variability of the interspike intervals in the fluctuation-driven regime (see the CV_{ISI}-$\langle I \rangle$ curve in Figure 3D).

Taking the data from Figures 2 and 3 together, the reduced bandwidth for GM in the configurations with NMDARs as compared to those without must result almost completely from differences in the input frequency–input current relationships. Because the presence of NMDARs enhances the total input current, the region where GM occurs is compressed to a narrower range of input frequencies. Furthermore, GM is also reduced by the saturation of NMDARs. This causes a decrease of gain at high input frequencies and can lead, as in configuration N128, to even a negative value of I_{GM} (see Figure 2D).

4 Discussion

We demonstrated in a cerebellar GC model receiving Poisson-distributed excitatory synaptic events that the input-output frequency relationship changes both in an additive and a multiplicative manner upon altering the level of shunting inhibition. This confirmed the general result that gain

changes can be induced by inhibition only (Murphy & Miller, 2003) and is in agreement with a recent study on the GC in which AMPAR excitation by MFs was simulated using a dynamic-clamp approach (Mitchell & Silver, 2003). The latter study showed clearly the possibility of GM due to shunting inhibition, where the strength of GM, that is, I_{GM}, was quite independent of the input frequency. In agreement herewith, we found only a relatively weak dependence of I_{GM} on the input frequency using only AMPARs. However, the inclusion of NMDARs led to a much stronger decrease of I_{GM} with input frequency, thereby reducing the bandwidth for GM. Moreover, the enhanced frequency dependence of I_{GM} and the enlarged variability of the ISIs (see Figure 3D) will make it more difficult for downstream neurons to process the signal (Salinas & Thier, 2000).

GM requires that the input to a neuron is highly variable, and it vanishes for a constant input current (Holt & Koch, 1997). The fact that the input of GCs consists of a small number of large-amplitude inputs is responsible for the high level of input noise. GM becomes less prominent for lower amplitudes of the EPSPs as in, for example, the model studied by Gabbiani et al. (1994), in which only an additive transformation on the application of shunting inhibition was found. In addition, their model NMDARs did not saturate, which resulted in a relatively larger role of the NMDAR-mediated currents.

In this study, we took into account both the direct and spillover component of synaptic activation, but their relative contributions were based on experimental data describing the situation after a single stimulus, as was also the case for the description of the relative contribution of synaptic and extrasynaptic NMDARs to the charge transfer (DiGregorio et al., 2002). However, it is not clear whether these single-stimulation data can be extrapolated to the case of high-frequency stimulation, because it is unlikely that glutamate concentrations within the glomerulus add linearly on subsequent stimuli. MF-GC synapses are densely packed within glomeruli, which are enwrapped by a glial sheath. Due to this structure, neurotransmitter concentrations can stay elevated for relatively long times. Spillover of glutamate by diffusion out of the synaptic cleft activates the low-affinity AMPARs of neighboring synapses in the glomerulus (DiGregorio et al., 2002). The spillover component of AMPAR activation contributes even more to the total charge transfer than the direct component. When activation of AMPARs or extrasynaptic NMDARs by spillover becomes more important during high-frequency stimulation, GM might be further reduced.

In our model, Mg^{2+} blocked and unblocked NMDARs instantaneously upon a voltage change. However, it has been shown recently (Kampa, Clements, Jonas, & Stuart, 2004) that only the Mg^{2+}-block occurs nearly instantaneously and that the kinetics of the Mg^{2+}-unblock contain both very fast ($\sim$100 μs) and slower components. With the instantaneous description of the Mg^{2+}-unblock, the contribution of NMDAR-mediated currents might

therefore be overestimated. The relative amplitudes of the slow unblock components depend, however, on the timing of glutamate release. Shortly after a glutamate pulse as well as during sustained glutamate release, the kinetics of the Mg^{2+}-unblock is dominated by the fast component (Kampa et al., 2004). Therefore, it is expected that a more realistic description of the Mg^{2+}-unblock would have only a minor influence on our results.

It has recently been suggested that shunting inhibition can enhance gain modulation in spatially extended neurons, especially when shunting inhibition targets the dendrite (Brizzi et al., 2004; Prescott & De Koninck, 2003). However, the soma and the dendrites of the GC are small, and the GC is under normal circumstances (without a large amount of shunting inhibition) electrotonically compact (D'Angelo et al., 1995; Silver et al., 1992). We verified that this was still the case in the presence of a high level of shunting inhibition by adding separate dendrites to the GC model. Although shunting inhibition increases the electrotonic length of the dendrites (Koch, 1999), the entire GC was almost isopotential, thereby validating a one-compartment description of the GC.

Cerebellar granule cells receive synapses from only four MFs on average, but because a unitary EPSP remains subthreshold (D'Angelo et al., 1995; Silver et al., 1992), correlated input is needed to evoke a spike. In accordance with this, in vivo granule cells have been reported to be almost silent (Chadderton, Margrie, & Hausser, 2004) while MFs spontaneously fire at high rates (Goldberg & Fernandez, 1971; Soja, Fragoso, Cairns, & Jia, 1996). The present model granule cell, having both AMPARs and NMDARs (our N64 case), fired in the presence of 1nS shunting inhibition at an average rate of 1.2 spikes per second during stimulation by four MFs firing each at a physiological resting rate of 25 spikes per second (Soja et al., 1996). From the cross-correlogram (not shown), the granule cell was assessed to fire on average on the arrival of four MF spikes above the background level within a narrow window of a few milliseconds. Shunting inhibition and an increase in the granule cell firing rate independently tended to sharpen the correlation peak. Although NMDARs would broaden the peak, this effect was small, and we never obtained broad correlation peaks like those observed in neurons that integrate many EPSPs from hundreds of weak synapses (Maex, Vos, & De Schutter, 2000).

Finally, reducing the degree of short-term correlation within the MF spike trains, by using a Poisson model with a 2 ms dead time (Eccles et al., 1971; Garwicz et al., 1998), did not affect our results. When individual MFs were modeled as a higher-order gamma process with a CV of the interspike interval of 0.68 (range 0.68–1.28 in Soja et al., 1996), the firing rate of the granule cell slightly decreased in the fluctuation-driven regime. In contrast, correlations between the MF input spike trains increase the fluctuations of the membrane potential (Fellous et al., 2003; Salinas & Sejnowski, 2002), resulting in an enhancement of the firing rate of the granule cell and its ISI variability.

From this, the cerebellar granule cell appears to behave primarily as a coincidence detector, driven by the synchronous activation of a few, strong synapses. The very high conduction velocity of the afferent pathways, like the dorsal spinocerebellar tract (80 m/s, Soja et al., 1996), supports this function. Shunting inhibition is able to control the coincidence threshold, and hence the granule cell firing rate, albeit on a slower timescale than the gain control function assigned originally by Marr (1969) to inhibition by Golgi cells.

Acknowledgments

References

Brizzi, L., Meunier, C., Zytnicki, D., Donnet, M., Hansel, D., D'Incamps, B. L., & Van Vreeswijk, C. (2004). How shunting inhibition affects the discharge of lumbar motoneurones: A dynamic clamp study in anaesthetized cats. *J. Physiol., 558*(Pt. 2), 671–683.

Bugmann, G. (1991). Summation and multiplication: Two distinct operation domains of leaky integrate-and-fire neurons. *Network, 2*, 489–509.

Burkitt, A. N., Meffin, H., & Grayden, D. B. (2003). Study of neuronal gain in a conductance-based leaky integrate-and-fire neuron model with balanced excitatory and inhibitory synaptic input. *Biol. Cybern., 89*(2), 119–125.

Cathala, L., Brickley, S., Cull-Candy, S., & Farrant, M. (2003). Maturation of EPSCs and intrinsic membrane properties enhances precision at a cerebellar synapse. *J. Neurosci., 23*(14), 6074–6085.

Chadderton, P., Margrie, T. W., & Hausser, M. (2004). Integration of quanta in cerebellar granule cells during sensory processing. *Nature, 428*(6985), 856–860.

Chance, F. S., Abbott, L. F., & Reyes, A. D. (2002). Gain modulation from background synaptic input. *Neuron, 35*(4), 773–782.

D'Angelo, E., De Filippi, G., Rossi, P., & Taglietti, V. (1995). Synaptic excitation of individual rat cerebellar granule cells in situ: Evidence for the role of NMDA receptors. *J. Physiol., 484* (Pt. 2), 397–413.

D'Angelo, E., Nieus, T., Maffei, A., Armano, S., Rossi, P., Taglietti, V., Fontana, A., & Naldi, G. (2001). Theta-frequency bursting and resonance in cerebellar granule cells: Experimental evidence and modeling of a slow K^+-dependent mechanism. *J. Neurosci., 21*(3), 759–770.

D'Angelo, E., Rossi, P., Armano, S., & Taglietti, V. (1999). Evidence for NMDA and mGlu receptor-dependent long-term potentiation of mossy fiber-granule cell transmission in rat cerebellum. *J. Neurophysiol., 81*(1), 277–287.

D'Angelo, E., Rossi, P., & Taglietti, V. (1993). Different proportions of N-methyl-D-aspartate and non-N-methyl-D-aspartate receptor currents at the mossy fibre-granule cell synapse of developing rat cerebellum. *Neuroscience, 53*(1), 121–130.

D'Angelo, E., Rossi, P., & Taglietti, V. (1994). Voltage-dependent kinetics of N-methyl-D-aspartate synaptic currents in rat cerebellar granule cells. *Eur. J. Neurosci., 6*(4), 640–645.

De Schutter, E. (2002). Cerebellar cortex: Computation by extrasynaptic inhibition. *Current Biology, 12*, R363–R365.

DiGregorio, D. A., Nusser, Z., & Silver, R. A. (2002). Spillover of glutamate onto synaptic AMPA receptors enhances fast transmission at a cerebellar synapse. *Neuron, 35*(3), 521–533.

Doiron, B., Longtin, A., Berman, N., & Maler, L. (2000). Subtractive and divisive inhibition: Effect of voltage-dependent inhibitory conductances and noise. *Neural Comput., 13*, 227–248.

Drew, P. J., & Abbott, L. F. (2003). Model of song selectivity and sequence generation in area HVc of the songbird. *J. Neurophysiol., 89*(5), 2697–2706.

Eccles, J. C., Faber, D. S., Murphy, J. T., Sabah, N. H., & Taborikova, H. (1971). Afferent volleys in limb nerves influencing impulse discharges in cerebellar cortex. I. In mossy fibers and granule cells. *Exp. Brain Res., 13*(1), 15–35.

Fellous, J. M., Rudolph, M., Destexhe, A., & Sejnowski, T. J. (2003). Synaptic background noise controls the input/output characteristics of single cells in an in vitro model of in vivo activity. *Neuroscience, 122*(3), 811–829.

Gabbiani, F., Midtgaard, J., & Knopfel, T. (1994). Synaptic integration in a model of cerebellar granule cells. *J. Neurophysiol., 72*(2), 999–1009.

Garwicz, M., Jorntell, H., & Ekerot, C. F. (1998). Cutaneous receptive fields and topography of mossy fibres and climbing fibres projecting to cat cerebellar C3 zone. *J. Physiol., 512* (Pt. 1), 277–293.

Goldberg, J. M., & Fernandez, C. (1971). Physiology of peripheral neurons innervating semicircular canals of the squirrel monkey. I. Resting discharge and response to constant angular accelerations. *J. Neurophysiol., 34*(4), 635–660.

Hamann, M., Rossi, D. J., & Attwell, D. (2002). Tonic and spillover inhibition of granule cells control information flow through cerebellar cortex. *Neuron, 33*(4), 625–633.

Hines, M. L., & Carnevale, N. T. (1997). The NEURON simulation environment. *Neural Comput., 9*(6), 1179–1209.

Holt, G. R., & Koch, C. (1997). Shunting inhibition does not have a divisive effect on firing rates. *Neural Comput., 9*(5), 1001–1013.

Ito, M. (1984). *The cerebellum and neural control*. New York: Raven Press.

Jahr, C. E., & Stevens, C. F. (1990). Voltage dependence of NMDA-activated macroscopic conductances predicted by single-channel kinetics. *J. Neurosci., 10*(9), 3178–3182.

Jakab, R. L., & Hamori, J. (1988). Quantitative morphology and synaptology of cerebellar glomeruli in the rat. *Anat. Embryol. (Berl.), 179*(1), 81–88.

Kampa, B. M., Clements, J., Jonas, P., & Stuart, G. J. (2004). Kinetics of Mg^{2+} unblock of NMDA receptors: Implications for spike-timing dependent synaptic plasticity. *J. Physiol., 556*(Pt. 2), 337–345.

Kase, M., Miller, D. C., & Noda, H. (1980). Discharges of Purkinje cells and mossy fibres in the cerebellar vermis of the monkey during saccadic eye movements and fixation. *J. Physiol., 300*, 539–555.

Koch, C. (1999). *Biophysics of computation*. New York: Oxford University Press.

Kuhn, A., Aertsen, A., & Rotter, S. (2004). Neuronal integration of synaptic input in the fluctuation-driven regime. *J. Neurosci., 24*(10), 2345–2356.

Maex, R., & De Schutter, E. (1998). Synchronization of golgi and granule cell firing in a detailed network model of the cerebellar granule cell layer. *J. Neurophysiol., 80*(5), 2521–2537.

Maex, R., Vos, B. P., & De Schutter, E. (2000). Weak common parallel fibre synapses explain the loose synchrony observed between rat cerebellar Golgi cells. *J. Physiol., 523*(Pt. 1), 175–192.

Marr, D. (1969). A theory of cerebellar cortex. *J. Physiol., 202*(2), 437–470.

Mitchell, S. J., & Silver, R. A. (2003). Shunting inhibition modulates neuronal gain during synaptic excitation. *Neuron, 38*(3), 433–445.

Murphy, B. K., & Miller, K. D. (2003). Multiplicative gain changes are induced by excitation or inhibition alone. *J. Neurosci., 23*(31), 10040–10051.

Prescott, S. A., & De Koninck, Y. (2003). Gain control of firing rate by shunting inhibition: Roles of synaptic noise and dendritic saturation. *Proc. Natl. Acad. Sci. USA, 100*(4), 2076–2081.

Ricciardi, L. M. (1977). *Diffusion processes and related topics in biology*. Berlin: Springer-Verlag.

Rice, S. O. (1954). Mathematical analysis of random noise. In N. Wax (Ed.), *Selected papers on noise and stochastic processes* (pp. 133–161). New York: Dover.

Rossi, D. J., Hamann, M., & Attwell, D. (2003). Multiple modes of GABAergic inhibition of rat cerebellar granule cells. *J. Physiol., 548*(Pt. 1), 97–110.

Rossi, P., De Filippi, G., Armano, S., Taglietti, V., & D'Angelo, E. (1998). The weaver mutation causes a loss of inward rectifier current regulation in premigratory granule cells of the mouse cerebellum. *J. Neurosci., 18*(10), 3537–3547.

Rossi, P., Sola, E., Taglietti, V., Borchardt, T., Steigerwald, F., Utvik, J. K., Ottersen, O. P., Kohr, G., & D'Angelo, E. (2002). NMDA receptor 2 (NR2) C-terminal control of NR open probability regulates synaptic transmission and plasticity at a cerebellar synapse. *J. Neurosci., 22*(22), 9687–9697.

Salinas, E., & Sejnowski, T. J. (2002). Integrate-and-fire neurons driven by correlated stochastic input. *Neural Comput., 14*(9), 2111–2155.

Salinas, E., & Thier, P. (2000). Gain modulation: A major computational principle of the central nervous system. *Neuron, 27*(1), 15–21.

Silver, R. A., Traynelis, S. F., & Cull-Candy, S. G. (1992). Rapid-time-course miniature and evoked excitatory currents at cerebellar synapses in situ. *Nature, 355*(6356), 163–166.

Soja, P. J., Fragoso, M. C., Cairns, B. E., & Jia, W. G. (1996). Dorsal spinocerebellar tract neurons in the chronic intact cat during wakefulness and sleep: Analysis of spontaneous spike activity. *J. Neurosci., 16*(3), 1260–1272.

Stein, R. B. (1965). A theoretical analysis of neuronal variability. *Biophys. J., 91*, 173–194.

Tiesinga, P. H., Jose, J. V., & Sejnowski, T. J. (2000). Comparison of current-driven and conductance-driven neocortical model neurons with Hodgkin-Huxley voltage-gated channels. *Phys. Rev. E Stat. Phys. Plasmas Fluids Relat. Interdiscip. Topics, 62*(6 Pt. B), 8413–8419.

Troyer, T. W., & Miller, K. D. (1997). Physiological gain leads to high ISI variability in a simple model of a cortical regular spiking cell. *Neural Comput., 9*(5), 971–983.

Tuckwell, H. C. (1988). *Introduction to theoretical neurobiology*. Cambridge: Cambridge University Press.

van Kampen, N. G. (1981). *Stochastic processes in physics and chemistry*. Amsterdam: North-Holland.

van Kan, P. L., Gibson, A. R., & Houk, J. C. (1993). Movement-related inputs to intermediate cerebellum of the monkey. *J. Neurophysiol., 69*(1), 74–94.

Wang, L. Y. (2000). The dynamic range for gain control of NMDA receptor-mediated synaptic transmission at a single synapse. *J. Neurosci., 20*(24), RC115.